

Contents lists available at [ScienceDirect](http://www.sciencedirect.com)

Journal of Quantitative Spectroscopy & Radiative Transfer

journal homepage: www.elsevier.com/locate/jqsrt

Decompositioning method to compute scattering by complex shaped particles using a multiple scattering **T**-matrix approach

Thomas Wriedt^a, Roman Schuh^{b,*}^a Institut für Werkstofftechnik, Badgasteiner Str. 3, 28359 Bremen, Germany^b FB4 Verfahrenstechnik, Universität Bremen, Badgasteiner Str. 3, 28359 Bremen, Germany

ARTICLE INFO

Article history:

Received 19 October 2007

Received in revised form

16 April 2008

Accepted 19 April 2008

Keywords:

Null-field method with discrete sources

T-matrix

Shape modeling

Multiple scattering

ABSTRACT

In a recent paper we proposed a decompositioning method to compute scattering by aggregated cylindrical fibres using a multiple scattering **T**-matrix approach. In this paper we extend this approach to scatterers lacking rotational symmetry. To investigate the capability of this method a square prism and a cube are decomposed into a number of subscatterers and scattering of the original particle shape is computed using multiple scattering. The results are validated using discrete dipole approximation (DDA).

© 2008 Elsevier Ltd. All rights reserved.

1. Introduction

The **T**-matrix method or null-field method is one of the most well-known light scattering theories to compute scattering by nonspherical particles. Recent reviews of the literature on this method have been published by Mishchenko et al. [1,2]. Computing light scattering by arbitrary shaped particles is an important subject in various scientific disciplines ranging from astrophysics to optical particle characterization. The well-known **T**-matrix method is of advantage because in a computed **T**-matrix all information on the scattering process is contained. Using a computed **T**-matrix orientational averaged scattering can easily be computed. Multiple scattering problems can be solved by combining the **T**-matrices of the different constituents. In multiple scattering by aggregates of particles, there was a focus on clusters of spheres until recently, although the method was extended to aggregates of rotationally symmetric particles by Peterson and Ström [3] in 1973 and a fast algorithm was published by Xu [4]. This theory was extended by Wriedt [5] to superellipsoids, and by Doicu et al. [10] to arbitrary shaped primary particles lacking rotational symmetry.

Thus more complicated scattering problems can be solved nowadays using the **T**-matrix approach. Examples of such scattering objects include recently developed nanoparticles, like nanohelices [6], nanobars [7], nanostars [8], nanocages, and nanoboxes [9].

The only restriction imposed on the scattering problem is that the circumscribed spheres of the scattering particles should not overlap. In investigating the problem of scattering by a nonspherical particle positioned on a plane interface, we found that we nonetheless got correct computational results if there is a small amount of overlap of the circumscribed sphere with the plane surface [11]. Thus the restriction of nonoverlapping of circumscribed spheres could be relaxed. In a recent paper on scattering by two crossed cylindrical fibres we further investigated this problem [12]. First computational

* Corresponding author.

E-mail addresses: thw@iwt.uni-bremen.de (T. Wriedt), schuh@iwt.uni-bremen.de (R. Schuh).

results on this scattering problem were originally presented in a recent review paper on the null-field method with discrete sources (NFM-DS) [14].

We proposed a decomposition method of the original scattering problem into a number of subscatterers and computing an approximation of original scattering problem using a multiple scattering approach combining the **T**-matrices of all subscatterers. We found that we got correct results up to a size parameter of 2.0. In this paper we like to extend the decomposition method to nonrotationally symmetric particles to further investigate the range of validity of the method.

The paper is divided as follows. First we present a short version of the multiple scattering theory based on our recent monograph [10]. Next we investigate the influence of the amount of overlapping of circumscribed spheres by varying the distance of a number of lined cubes. Then we investigate the capability of the method by varying the size parameter of a square prism decomposed into four cubes. Finally, we decompose a cube into eight cubes and compare the multiple scattering results to discrete dipole approximation (DDA) results.

2. T-matrix method

In this section we like to outline the basics of the null-field method for an arbitrary number of nonrotationally symmetric particles by using the translation properties of vector spherical wave functions. Our treatment closely follows the derivation given by Peterson and Ström [3,15]. The full theory together with all Fortran programs is published in a monograph by Doicu et al. [10]. For a full description of the theory the interested reader is referred to this book.

For the purpose of clarity of presentation we will first consider the case of two homogeneous particles in a homogeneous medium with a relative permittivity ϵ_s and a relative permeability μ_s . The scattering geometry of the two particles is shown in Fig. 1. The surfaces S_1 and S_2 of the particles are defined with respect to the particle coordinate systems $O_1x_1y_1z_1$ and $O_2x_2y_2z_2$, respectively, while the global coordinate system of the ensemble is denoted by $Oxyz$. The coordinate system $O_1x_1y_1z_1$ is obtained by translating the coordinate system $Oxyz$ through \mathbf{r}_{01} and by rotating the translated coordinate system through the Euler angles α_1, β_1 , and γ_1 . Similarly, the coordinate system $O_2x_2y_2z_2$ is obtained by translating the coordinate system $Oxyz$ through \mathbf{r}_{02} and by rotating the translated coordinate system through the Euler angles α_2, β_2 , and γ_2 . The electromagnetic boundary-value problem for the two scattering particles has the following formulation:

Given the external excitation $\mathbf{E}_e, \mathbf{H}_e$ as an entire solution to the Maxwell equations, find the scattered field $\mathbf{E}_s, \mathbf{H}_s$ and the internal fields $\mathbf{E}_{i,1}, \mathbf{H}_{i,1}$ and $\mathbf{E}_{i,2}, \mathbf{H}_{i,2}$ satisfying the Maxwell equations

$$\begin{aligned} \nabla \times \mathbf{E} &= jk_0\mu\mathbf{H}, \\ \nabla \times \mathbf{H} &= -jk_0\epsilon\mathbf{E} \end{aligned} \tag{1}$$

in $D_s, D_{i,1}$, and $D_{i,2}$, the boundary conditions

$$\begin{aligned} \mathbf{n} \times \mathbf{E}_i - \mathbf{n} \times \mathbf{E}_s &= \mathbf{n} \times \mathbf{E}_e, \\ \mathbf{n} \times \mathbf{H}_i - \mathbf{n} \times \mathbf{H}_s &= \mathbf{n} \times \mathbf{H}_e \end{aligned} \tag{2}$$

on S_1 and on S_2 , and the Silver–Müller radiation condition for the scattered field.

The Stratton–Chu representation theorem [10] for the scattered field \mathbf{E}_s in $D_{i,1}$ and $D_{i,2}$ together with the boundary (2) yields the general null-field equation

$$\begin{aligned} \mathbf{E}_e(\mathbf{r}) + \nabla \times \int_{S_1} \mathbf{e}_{i,1}(\mathbf{r}')g(k_s, \mathbf{r}, \mathbf{r}') dS(\mathbf{r}') + \frac{j}{k_0\epsilon_s} \nabla \times \nabla \times \int_{S_1} \mathbf{h}_{i,1}(\mathbf{r}')g(k_s, \mathbf{r}, \mathbf{r}') dS(\mathbf{r}') \\ + \nabla \times \int_{S_2} \mathbf{e}_{i,2}(\mathbf{r}'')g(k_s, \mathbf{r}, \mathbf{r}'') dS(\mathbf{r}'') + \frac{j}{k_0\epsilon_s} \nabla \times \nabla \times \int_{S_2} \mathbf{h}_{i,2}(\mathbf{r}'')g(k_s, \mathbf{r}, \mathbf{r}'') dS(\mathbf{r}'') = 0, \quad \mathbf{r} \in D_{i,1} \cup D_{i,2}. \end{aligned} \tag{3}$$

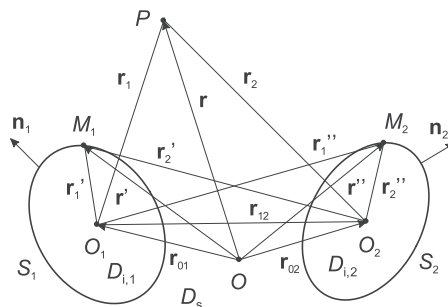


Fig. 1. Geometry of two scattering particles.

3. Expansion of the incident field

Before we derive the null-field equations, we will present the relation between the expansion coefficients a_v, b_v of the incident field in the global coordinate system $Oxyz$:

$$\mathbf{E}_e(\mathbf{r}) = \sum_v a_v \mathbf{M}_v^1(k_s \mathbf{r}) + b_v \mathbf{N}_v^1(k_s \mathbf{r}), \tag{4}$$

and the expansion coefficients $a_{1,v}, b_{1,v}$ of the incident field in the particle coordinate system $O_1x_1y_1z_1$,

$$\mathbf{E}_e(\mathbf{r}_1) = \sum_v a_{1,v} \mathbf{M}_v^1(k_s \mathbf{r}_1) + b_{1,v} \mathbf{N}_v^1(k_s \mathbf{r}_1). \tag{5}$$

For this purpose we choose a sufficiently large surface S enclosing O and O_1 (Fig. 2) and in each coordinate system we use the Stratton–Chu representation theorem for the incident field in the interior of S . We obtain

$$\begin{pmatrix} a_v \\ b_v \end{pmatrix} = -\frac{jk_s^2}{\pi} \int_S \left[\mathbf{e}_e(\mathbf{r}') \begin{pmatrix} \mathbf{N}_v^3(k_s \mathbf{r}') \\ \mathbf{M}_v^3(k_s \mathbf{r}') \end{pmatrix} + j\sqrt{\frac{\mu_s}{\epsilon_s}} \mathbf{h}_e(\mathbf{r}') \begin{pmatrix} \mathbf{M}_v^3(k_s \mathbf{r}') \\ \mathbf{N}_v^3(k_s \mathbf{r}') \end{pmatrix} \right] dS(\mathbf{r}') \tag{6}$$

in the global coordinate system and

$$\begin{pmatrix} a_{1,v} \\ b_{1,v} \end{pmatrix} = -\frac{jk_s^2}{\pi} \int_S \left[\mathbf{e}_e(\mathbf{r}'_1) \begin{pmatrix} \mathbf{N}_v^3(k_s \mathbf{r}'_1) \\ \mathbf{M}_v^3(k_s \mathbf{r}'_1) \end{pmatrix} + j\sqrt{\frac{\mu_s}{\epsilon_s}} \mathbf{h}_e(\mathbf{r}'_1) \begin{pmatrix} \mathbf{M}_v^3(k_s \mathbf{r}'_1) \\ \mathbf{N}_v^3(k_s \mathbf{r}'_1) \end{pmatrix} \right] dS(\mathbf{r}'_1), \tag{7}$$

respectively, in the local coordinate system. Using the addition theorem for radiating vector spherical wave functions:

$$\begin{bmatrix} \mathbf{M}_v^3(k_s \mathbf{r}'_1) \\ \mathbf{N}_v^3(k_s \mathbf{r}'_1) \end{bmatrix} = [(\mathcal{S}_{10}^{rt})_{v\mu}] \begin{bmatrix} \mathbf{M}_\mu^3(k_s \mathbf{r}') \\ \mathbf{N}_\mu^3(k_s \mathbf{r}') \end{bmatrix}, \tag{8}$$

where the transformation matrix \mathcal{S}_{10}^{rt} is a product of a translation and a rotation matrix:

$$\mathcal{S}_{10}^{rt} = \mathcal{R}(-\gamma_1, -\beta_1, -\alpha_1) \mathcal{T}^{33}(-k_s \mathbf{r}_{01}) \quad \text{for } r' > r_{01}, \tag{9}$$

and taking into account that the transformation matrix \mathcal{S}_{10}^{rt} is a block-symmetric matrix, yields the relation of the expansion coefficients of the incident field in the particle coordinate system $O_1x_1y_1z_1$ to the expansion coefficients of the incident field in the global coordinate system $Oxyz$:

$$\begin{bmatrix} a_{1,v} \\ b_{1,v} \end{bmatrix} = [(\mathcal{S}_{10}^{rt})_{v\mu}] \begin{bmatrix} a_\mu \\ b_\mu \end{bmatrix}. \tag{10}$$

The condition $r' > r_{01}$ can always be satisfied in practice by an appropriate choice of the auxiliary surface S , whence, using the identity $\mathcal{T}^{33}(-k_s \mathbf{r}_{01}) = \mathcal{T}^{11}(-k_s \mathbf{r}_{01})$, we see that the transformation matrix \mathcal{S}_{10}^{rt} is given by

$$\mathcal{S}_{10}^{rt} = \mathcal{R}(-\gamma_1, -\beta_1, -\alpha_1) \mathcal{T}^{11}(-k_s \mathbf{r}_{01}). \tag{11}$$

4. Two-particle problem

In this section we like first to derive the **T**-matrix of the two-particle system. We start with deriving the set of null-field equations needed in the following. Passing from the origin O to the origin O_1 , using the following relations for the Green function:

$$\begin{aligned} g(k_s, \mathbf{r}, \mathbf{r}') &= g(k_s, \mathbf{r}_1, \mathbf{r}'_1), \\ g(k_s, \mathbf{r}, \mathbf{r}'') &= g(k_s, \mathbf{r}_1, \mathbf{r}''_1), \end{aligned} \tag{12}$$

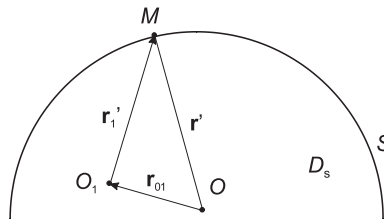


Fig. 2. Auxiliary surface S .

and restricting \mathbf{r}_1 to lie on a sphere enclosed in $D_{i,1}$, gives the null-field equations in $D_{i,1}$:

$$\begin{aligned} & \frac{jk_s^2}{\pi} \int_{S_1} \left[\mathbf{e}_{i,1}(\mathbf{r}'_1) \cdot \begin{pmatrix} \mathbf{N}_v^3(k_s \mathbf{r}'_1) \\ \mathbf{M}_v^3(k_s \mathbf{r}'_1) \end{pmatrix} + j\sqrt{\frac{\mu_s}{\epsilon_s}} \mathbf{h}_{i,1}(\mathbf{r}'_1) \cdot \begin{pmatrix} \mathbf{M}_v^3(k_s \mathbf{r}'_1) \\ \mathbf{N}_v^3(k_s \mathbf{r}'_1) \end{pmatrix} \right] dS(\mathbf{r}'_1) \\ & + \frac{jk_s^2}{\pi} \int_{S_2} \left[\mathbf{e}_{i,2}(\mathbf{r}'_2) \cdot \begin{pmatrix} \mathbf{N}_v^3(k_s \mathbf{r}'_2) \\ \mathbf{M}_v^3(k_s \mathbf{r}'_2) \end{pmatrix} + j\sqrt{\frac{\mu_s}{\epsilon_s}} \mathbf{h}_{i,2}(\mathbf{r}'_2) \cdot \begin{pmatrix} \mathbf{M}_v^3(k_s \mathbf{r}'_2) \\ \mathbf{N}_v^3(k_s \mathbf{r}'_2) \end{pmatrix} \right] dS(\mathbf{r}'_2) = - \begin{pmatrix} a_{1,v} \\ b_{1,v} \end{pmatrix}, \quad v = 1, 2, \dots \end{aligned} \quad (13)$$

where the identities $\mathbf{e}_{i,2}(\mathbf{r}'_2) = \mathbf{e}_{i,2}(\mathbf{r}'_1)$ and $\mathbf{h}_{i,2}(\mathbf{r}'_2) = \mathbf{h}_{i,2}(\mathbf{r}'_1)$ have been used. For the general null-field equation in $D_{i,2}$ we proceed analogously but restrict \mathbf{r}_2 to lie on a sphere enclosed in $D_{i,2}$. We obtain

$$\begin{aligned} & \frac{jk_s^2}{\pi} \int_{S_1} \left[\mathbf{e}_{i,1}(\mathbf{r}'_1) \cdot \begin{pmatrix} \mathbf{N}_v^3(k_s \mathbf{r}'_2) \\ \mathbf{M}_v^3(k_s \mathbf{r}'_2) \end{pmatrix} + j\sqrt{\frac{\mu_s}{\epsilon_s}} \mathbf{h}_{i,1}(\mathbf{r}'_1) \cdot \begin{pmatrix} \mathbf{M}_v^3(k_s \mathbf{r}'_2) \\ \mathbf{N}_v^3(k_s \mathbf{r}'_2) \end{pmatrix} \right] dS(\mathbf{r}'_1) \\ & + \frac{jk_s^2}{\pi} \int_{S_2} \left[\mathbf{e}_{i,2}(\mathbf{r}'_2) \cdot \begin{pmatrix} \mathbf{N}_v^3(k_s \mathbf{r}'_2) \\ \mathbf{M}_v^3(k_s \mathbf{r}'_2) \end{pmatrix} + j\sqrt{\frac{\mu_s}{\epsilon_s}} \mathbf{h}_{i,2}(\mathbf{r}'_2) \cdot \begin{pmatrix} \mathbf{M}_v^3(k_s \mathbf{r}'_2) \\ \mathbf{N}_v^3(k_s \mathbf{r}'_2) \end{pmatrix} \right] dS(\mathbf{r}'_2) = - \begin{pmatrix} a_{2,v} \\ b_{2,v} \end{pmatrix}, \quad v = 1, 2, \dots \end{aligned} \quad (14)$$

where, as before, we have taken into account that $\mathbf{e}_{i,1}(\mathbf{r}'_1) = \mathbf{e}_{i,1}(\mathbf{r}'_2)$ and $\mathbf{h}_{i,1}(\mathbf{r}'_1) = \mathbf{h}_{i,1}(\mathbf{r}'_2)$.

The surface fields $\mathbf{e}_{i,1}$, $\mathbf{h}_{i,1}$ and $\mathbf{e}_{i,2}$, $\mathbf{h}_{i,2}$ are the tangential components of the electric and magnetic fields in the domains $D_{i,1}$ and $D_{i,2}$, respectively, and the surface field approximations can be expressed as linear combinations of regular vector spherical wave functions:

$$\begin{pmatrix} \mathbf{e}_{i,1}^N(\mathbf{r}'_1) \\ \mathbf{h}_{i,1}^N(\mathbf{r}'_1) \end{pmatrix} = \sum_{\mu=1}^N c_{1,\mu}^N \begin{pmatrix} \mathbf{n}_1(\mathbf{r}'_1) \times \mathbf{M}_\mu^1(k_{i,1} \mathbf{r}'_1) \\ -j\sqrt{\frac{\epsilon_{i,1}}{\mu_{i,1}}} \mathbf{n}_1(\mathbf{r}'_1) \times \mathbf{N}_\mu^1(k_{i,1} \mathbf{r}'_1) \end{pmatrix} + d_{1,\mu}^N \begin{pmatrix} \mathbf{n}_1(\mathbf{r}'_1) \times \mathbf{N}_\mu^1(k_{i,1} \mathbf{r}'_1) \\ -j\sqrt{\frac{\epsilon_{i,1}}{\mu_{i,1}}} \mathbf{n}_1(\mathbf{r}'_1) \times \mathbf{M}_\mu^1(k_{i,1} \mathbf{r}'_1) \end{pmatrix} \quad (15)$$

and

$$\begin{pmatrix} \mathbf{e}_{i,2}^N(\mathbf{r}'_2) \\ \mathbf{h}_{i,2}^N(\mathbf{r}'_2) \end{pmatrix} = \sum_{\mu=1}^N c_{2,\mu}^N \begin{pmatrix} \mathbf{n}_2(\mathbf{r}'_2) \times \mathbf{M}_\mu^1(k_{i,2} \mathbf{r}'_2) \\ -j\sqrt{\frac{\epsilon_{i,2}}{\mu_{i,2}}} \mathbf{n}_2(\mathbf{r}'_2) \times \mathbf{N}_\mu^1(k_{i,2} \mathbf{r}'_2) \end{pmatrix} + d_{2,\mu}^N \begin{pmatrix} \mathbf{n}_2(\mathbf{r}'_2) \times \mathbf{N}_\mu^1(k_{i,2} \mathbf{r}'_2) \\ -j\sqrt{\frac{\epsilon_{i,2}}{\mu_{i,2}}} \mathbf{n}_2(\mathbf{r}'_2) \times \mathbf{M}_\mu^1(k_{i,2} \mathbf{r}'_2) \end{pmatrix}. \quad (16)$$

Inserting these expansions (15) and (16) into the null-field equations (13) and (14), using the addition theorem for vector spherical wave functions

$$\begin{bmatrix} \mathbf{M}_v^3(k_s \mathbf{r}'_1) \\ \mathbf{N}_v^3(k_s \mathbf{r}'_1) \end{bmatrix} = [(\tilde{\mathcal{S}}_{12}^{\text{tr}})_{v\mu}] \begin{bmatrix} \mathbf{M}_\mu^1(k_s \mathbf{r}'_2) \\ \mathbf{N}_\mu^1(k_s \mathbf{r}'_2) \end{bmatrix}, \quad (17)$$

with

$$\tilde{\mathcal{S}}_{12}^{\text{tr}} = \mathcal{A}(-\gamma_1, -\beta_1, -\alpha_1) \mathcal{F}^{31}(k_s \mathbf{r}_{12}) \mathcal{A}(\alpha_2, \beta_2, \gamma_2) \quad \text{for } r'_2 < r_{12}, \quad (18)$$

and

$$\begin{bmatrix} \mathbf{M}_v^3(k_s \mathbf{r}'_2) \\ \mathbf{N}_v^3(k_s \mathbf{r}'_2) \end{bmatrix} = [(\tilde{\mathcal{S}}_{21}^{\text{tr}})_{v\mu}] \begin{bmatrix} \mathbf{M}_\mu^1(k_s \mathbf{r}'_1) \\ \mathbf{N}_\mu^1(k_s \mathbf{r}'_1) \end{bmatrix}, \quad (19)$$

with

$$\tilde{\mathcal{S}}_{21}^{\text{tr}} = \mathcal{A}(-\gamma_2, -\beta_2, -\alpha_2) \mathcal{F}^{31}(-k_s \mathbf{r}_{12}) \mathcal{A}(\alpha_1, \beta_1, \gamma_1) \quad \text{for } r'_1 < r_{12}, \quad (20)$$

and taking into account the transformation rule for the incident field coefficients (10) yield the system of matrix equations

$$\begin{aligned} \mathbf{Q}_1^{31}(k_s, k_{i,1}) \mathbf{i}_1 + \tilde{\mathcal{S}}_{12}^{\text{tr}} \mathbf{Q}_2^{11}(k_s, k_{i,2}) \mathbf{i}_2 &= -\mathcal{S}_{10}^{\text{tr}} \mathbf{e}, \\ \tilde{\mathcal{S}}_{21}^{\text{tr}} \mathbf{Q}_1^{11}(k_s, k_{i,1}) \mathbf{i}_1 + \mathbf{Q}_2^{31}(k_s, k_{i,2}) \mathbf{i}_2 &= -\mathcal{S}_{20}^{\text{tr}} \mathbf{e}, \end{aligned} \quad (21)$$

where $\mathbf{i}_1 = [c_{1,\mu}^N, d_{1,\mu}^N]^T$, $\mathbf{i}_2 = [c_{2,\mu}^N, d_{2,\mu}^N]^T$ and, as usual, $\mathbf{e} = [a_v, b_v]^T$ is the vector containing the expansion coefficients of the incident field in the global coordinate system. Further, defining the scattered-field coefficients,

$$\begin{aligned} \mathbf{s}_1 &= \mathbf{Q}_1^{11}(k_s, k_{i,1}) \mathbf{i}_1, \\ \mathbf{s}_2 &= \mathbf{Q}_2^{11}(k_s, k_{i,2}) \mathbf{i}_2, \end{aligned} \quad (22)$$

and introducing the individual transition matrices,

$$\begin{aligned}\mathbf{T}_1 &= -\mathbf{Q}_1^{11}(k_s, k_{i,1})[\mathbf{Q}_1^{31}(k_s, k_{i,1})]^{-1}, \\ \mathbf{T}_2 &= -\mathbf{Q}_2^{11}(k_s, k_{i,2})[\mathbf{Q}_2^{31}(k_s, k_{i,2})]^{-1},\end{aligned}\quad (23)$$

we can rewrite the matrix system (21) as

$$\begin{aligned}\mathbf{s}_1 - \mathbf{T}_1 \tilde{\mathcal{S}}_{12}^{\text{trr}} \mathbf{s}_2 &= \mathbf{T}_1 \mathcal{S}_{10}^{\text{tr}} \mathbf{e}, \\ \mathbf{s}_2 - \mathbf{T}_2 \tilde{\mathcal{S}}_{21}^{\text{trr}} \mathbf{s}_1 &= \mathbf{T}_2 \mathcal{S}_{20}^{\text{tr}} \mathbf{e},\end{aligned}\quad (24)$$

and thus find the solutions for the scattered-field coefficients

$$\begin{aligned}\mathbf{s}_1 &= \mathbf{T}_1 (\mathbf{I} - \tilde{\mathcal{S}}_{12}^{\text{trr}} \mathbf{T}_2 \tilde{\mathcal{S}}_{21}^{\text{trr}} \mathbf{T}_1)^{-1} (\mathcal{S}_{10}^{\text{tr}} + \tilde{\mathcal{S}}_{12}^{\text{trr}} \mathbf{T}_2 \mathcal{S}_{20}^{\text{tr}}), \\ \mathbf{s}_2 &= \mathbf{T}_2 (\mathbf{I} - \tilde{\mathcal{S}}_{21}^{\text{trr}} \mathbf{T}_1 \tilde{\mathcal{S}}_{12}^{\text{trr}} \mathbf{T}_2)^{-1} (\mathcal{S}_{20}^{\text{tr}} + \tilde{\mathcal{S}}_{21}^{\text{trr}} \mathbf{T}_1 \mathcal{S}_{10}^{\text{tr}}).\end{aligned}\quad (25)$$

To compute the \mathbf{T} -matrix of the two-particle system and to derive a scattered-field expansion centred at the origin Oxy of the global coordinate system, we use the Stratton–Chu representation theorem for the scattered field \mathbf{E}_s in D_s . In the exterior of a sphere enclosing the two particles, the expansion of the approximate scattered field \mathbf{E}_s^N in terms of radiating vector spherical wave functions reads as

$$\mathbf{E}_s^N(\mathbf{r}t) = \sum_{v=1}^N f_v^N \mathbf{M}_v^3(k_s \mathbf{r}) + g_v^N \mathbf{N}_v^3(k_s \mathbf{r}), \quad (26)$$

where the expansion coefficients $\mathbf{s} = [f_v^N, g_v^N]^T$ are given by

$$\begin{aligned}\begin{pmatrix} f_v^N \\ g_v^N \end{pmatrix} &= \frac{jk_s^2}{\pi} \int_{S_1} \left[\mathbf{e}_{i,1}^N(\mathbf{r}'_1) \begin{pmatrix} \mathbf{N}_v^1(k_s \mathbf{r}') \\ \mathbf{M}_v^1(k_s \mathbf{r}') \end{pmatrix} + j \sqrt{\frac{\mu_s}{\varepsilon_s}} \mathbf{h}_{i,1}^N(\mathbf{r}'_1) \begin{pmatrix} \mathbf{M}_v^1(k_s \mathbf{r}') \\ \mathbf{N}_v^1(k_s \mathbf{r}') \end{pmatrix} \right] dS(\mathbf{r}'_1) \\ &+ \frac{jk_s^2}{\pi} \int_{S_2} \left[\mathbf{e}_{i,2}^N(\mathbf{r}'_2) \begin{pmatrix} \mathbf{N}_v^1(k_s \mathbf{r}'') \\ \mathbf{M}_v^1(k_s \mathbf{r}'') \end{pmatrix} + j \sqrt{\frac{\mu_s}{\varepsilon_s}} \mathbf{h}_{i,2}^N(\mathbf{r}'_2) \begin{pmatrix} \mathbf{M}_v^1(k_s \mathbf{r}'') \\ \mathbf{N}_v^1(k_s \mathbf{r}'') \end{pmatrix} \right] dS(\mathbf{r}'_2).\end{aligned}\quad (27)$$

Finally, using the addition theorem for the regular vector spherical wave functions,

$$\begin{bmatrix} \mathbf{M}_v^1(k_s \mathbf{r}') \\ \mathbf{N}_v^1(k_s \mathbf{r}') \end{bmatrix} = [(\mathcal{S}_{01}^{\text{tr}})_{v\bar{\mu}}] \begin{bmatrix} \mathbf{M}_{\bar{\mu}}^1(k_s \mathbf{r}'_1) \\ \mathbf{N}_{\bar{\mu}}^1(k_s \mathbf{r}'_1) \end{bmatrix}, \quad (28)$$

with the transformation matrix $\mathcal{S}_{01}^{\text{tr}}$ given as a product of a translation and a rotation matrix

$$\mathcal{S}_{01}^{\text{tr}} = \mathcal{T}^{11}(k_s \mathbf{r}_{01}) \mathcal{R}(\alpha_1, \beta_1, \gamma_1), \quad (29)$$

and

$$\begin{bmatrix} \mathbf{M}_v^1(k_s \mathbf{r}'') \\ \mathbf{N}_v^1(k_s \mathbf{r}'') \end{bmatrix} = [(\mathcal{S}_{02}^{\text{tr}})_{v\bar{\mu}}] \begin{bmatrix} \mathbf{M}_{\bar{\mu}}^1(k_s \mathbf{r}'_2) \\ \mathbf{N}_{\bar{\mu}}^1(k_s \mathbf{r}'_2) \end{bmatrix}, \quad (30)$$

with

$$\mathcal{S}_{02}^{\text{tr}} = \mathcal{T}^{11}(k_s \mathbf{r}_{02}) \mathcal{R}(\alpha_2, \beta_2, \gamma_2), \quad (31)$$

we obtain the expansion coefficients of the scattered field

$$\begin{aligned}\mathbf{s} &= \mathcal{S}_{01}^{\text{tr}} \mathbf{Q}_1^{11}(k_s, k_{i,1}) \mathbf{i}_1 + \mathcal{S}_{02}^{\text{tr}} \mathbf{Q}_2^{11}(k_s, k_{i,2}) \mathbf{i}_2 \\ &= \mathcal{S}_{01}^{\text{tr}} \mathbf{s}_1 + \mathcal{S}_{02}^{\text{tr}} \mathbf{s}_2,\end{aligned}\quad (32)$$

where $\mathbf{s} = [f_v^N, g_v^N]^T$ is the vector containing the expansion coefficients of the scattered field in the global coordinate system. Combining (25) and (32), and using the identities $\mathcal{S}_{20}^{\text{tr}} (\mathcal{S}_{10}^{\text{tr}})^{-1} = \mathcal{S}_{21}^{\text{trr}}$ and $\mathcal{S}_{10}^{\text{tr}} (\mathcal{S}_{20}^{\text{tr}})^{-1} = \mathcal{S}_{12}^{\text{trr}}$, yields the \mathbf{T} -matrix [3]

$$\mathbf{T} = \mathcal{S}_{01}^{\text{tr}} \mathbf{T}_1 (\mathbf{I} - \tilde{\mathcal{S}}_{12}^{\text{trr}} \mathbf{T}_2 \tilde{\mathcal{S}}_{21}^{\text{trr}} \mathbf{T}_1)^{-1} (\mathbf{I} + \tilde{\mathcal{S}}_{12}^{\text{trr}} \mathbf{T}_2 \mathcal{S}_{21}^{\text{trr}}) \mathcal{S}_{10}^{\text{tr}} + \mathcal{S}_{02}^{\text{tr}} \mathbf{T}_2 (\mathbf{I} - \tilde{\mathcal{S}}_{21}^{\text{trr}} \mathbf{T}_1 \tilde{\mathcal{S}}_{12}^{\text{trr}} \mathbf{T}_2)^{-1} (\mathbf{I} + \tilde{\mathcal{S}}_{21}^{\text{trr}} \mathbf{T}_1 \mathcal{S}_{12}^{\text{trr}}) \mathcal{S}_{20}^{\text{tr}}, \quad (33)$$

where the explicit expressions of the transformation matrices $\mathcal{S}_{21}^{\text{trr}}$ and $\mathcal{S}_{12}^{\text{trr}}$ are given by

$$\mathcal{S}_{12}^{\text{trr}} = \mathcal{R}(-\gamma_1, -\beta_1, -\alpha_1) \mathcal{T}^{11}(k_s \mathbf{r}_{12}) \mathcal{R}(\alpha_2, \beta_2, \gamma_2) \quad (34)$$

and

$$\mathcal{S}_{21}^{\text{rtt}} = \mathcal{R}(-\gamma_2, -\beta_2, -\alpha_2) \mathcal{F}^{-11}(-k_s \mathbf{r}_{12}) \mathcal{R}(\alpha_1, \beta_1, \gamma_1), \quad (35)$$

respectively, where \mathcal{F} and \mathcal{R} are defined in Appendix B of Doicu et al. [10]. Eq. (33) gives the system transition matrix \mathbf{T} in terms of the individual transition matrices \mathbf{T}_1 and \mathbf{T}_2 and the transformation matrices \mathcal{S} and $\tilde{\mathcal{S}}$. The transformation matrices \mathcal{S} and $\tilde{\mathcal{S}}$ involve translations of the regular and radiating vector spherical wave functions, respectively, and geometric constraints are introduced by the $\tilde{\mathcal{S}}$ matrices.

5. \mathcal{N} particle generalization

The generalization of the \mathbf{T} -matrix relation to a system with more than two constituent particles is presented next. The system of matrix equations consists in the null-field equations in the interior of all particles S_l :

$$\mathbf{s}_l - \mathbf{T}_l \sum_{p \neq l}^{\mathcal{N}} \tilde{\mathcal{S}}_{lp}^{\text{rtt}} \mathbf{s}_p = \mathbf{T}_l \mathcal{S}_{l0}^{\text{rt}} \mathbf{e} \quad \text{for } l = 1, 2, \dots, \mathcal{N}, \quad (36)$$

and the matrix equation corresponding to the scattered-field representation

$$\mathbf{s} = \sum_{l=1}^{\mathcal{N}} \mathcal{S}_{0l}^{\text{tr}} \mathbf{s}_l. \quad (37)$$

In a practical computer implementation it is appropriate to consider the global matrix \mathbf{A} with block-matrix components given by

$$\begin{aligned} \mathbf{A}^{ll} &= \mathbf{I}, \quad l = 1, 2, \dots, \mathcal{N}, \\ \mathbf{A}^{lp} &= -\mathbf{T}_l \tilde{\mathcal{S}}_{lp}^{\text{rtt}}, \quad l \neq p, \quad l, p = 1, 2, \dots, \mathcal{N}, \end{aligned} \quad (38)$$

and to express the solution to the system of matrix equations (36) as

$$\mathbf{s}_l = \left(\sum_{p=1}^{\mathcal{N}} \mathcal{A}^{lp} \mathbf{T}_p \mathcal{S}_{p0}^{\text{rt}} \right) \mathbf{e}, \quad l = 1, 2, \dots, \mathcal{N}, \quad (39)$$

where \mathcal{A} stands for \mathbf{A}^{-1} and \mathcal{A}^{lp} , $l, p = 1, 2, \dots, \mathcal{N}$, are the block-matrix components of \mathcal{A} . In view of the scattered-field representation (37), the system \mathbf{T} -matrix becomes

$$\mathbf{T} = \sum_{l=1}^{\mathcal{N}} \sum_{p=1}^{\mathcal{N}} \mathcal{S}_{0l}^{\text{tr}} \mathcal{A}^{lp} \mathbf{T}_p \mathcal{S}_{p0}^{\text{rt}}, \quad (40)$$

and this transition matrix can be used to compute the scattering characteristics for fixed or random orientations of an ensemble of arbitrarily shaped nonrotationally symmetric particles.

From the \mathbf{T} -matrix the scattered field (26) and all other scattering quantities can be computed. Especially for plotting the scattering diagrams shown in the next section, we compute the differential scattering cross-section (DSCS) for p- and s-incident polarization from the far field pattern, that is, vector field given on the unit sphere $\mathbf{E}_{s\infty}$:

$$\text{DSCS} = |\mathbf{E}_{s\infty}|^2. \quad (41)$$

6. Simulation results

In this section we like to investigate the capability of the decomposition method by computing scattering by particles decomposed into a number of cubes and comparing results to results obtained using the discrete dipole approximation (DDA). The main \mathbf{T} -matrix programs used are also published on CD with the monograph by Doicu et al. [10]. The first computational step involves the calculation of the individual \mathbf{T} -matrix of the basic cube by using the TNONAXSYM routine. The individual \mathbf{T} -matrices are then used to compute the \mathbf{T} -matrix of the composite particle using multiple scattering with the TMULT routine. In our exemplary simulations for the nonaxisymmetric particles, we additionally use the program DDSCAT by Draine and Flatau [13] for the numerical comparison of the results. The program DDSCAT utilizes the method of DDA for the computation of the light scattering by arbitrary shaped particles. The examined particle shapes are already included with DDSCAT. The generation of a model of two separated cubes is possible in DDSCAT with the built-in routine BLOCKS.

For the analysis of the deviations in the DSCS between the different configurations we use a root mean square (RMS) value which is defined by

$$\text{RMS}(\text{DSCS}_1, \text{DSCS}_2) = \sqrt{\frac{1}{181} \sum_{i=1}^{181} (\log \text{DSCS}_1(i) - \log \text{DSCS}_2(i))^2}, \quad (42)$$

where DSCS_1 and DSCS_2 denote the respective DSCSs in the scattering plane ($0^\circ < \theta < 180^\circ$, $\varphi = 0^\circ$).

In the following we present scattering computational results for nonaxisymmetric particles which can be composed of basic cubes. At first, we show scattering computations for two attached cubes and investigate the deviations arising from the overlapping circumscribing spheres in dependence on the separation distance of the two cubes. The next example is a square prism composed of four basic cubes. Here, we show the computed scattering distributions for different sizes and the corresponding RMS errors. Finally, we present computational results for a cube consisting of eight basic cubes, where the circumscribing spheres of the single cubes intersect heavily with neighbouring spheres. In this case, the errors are expected to be higher compared to the other examples.

The size of the examined particle is varied in a wide range whereas the aspect ratio is kept constant. The range of the size parameter of the basic cubes is from $kd = 0.5$ up to $kd = 8.0$, where $k = 2\pi/\lambda$ is the wavenumber and d is the edge length of the basic cube. The wavelength of the incident plane wave is fixed at $\lambda = 2\pi/10$. In all computations we use a refractive index of $1.5 + 0.0i$.

6.1. Square prism built-up of two cubes

In order to investigate the validity of the method of multiple scattering by nonaxisymmetric particles, we compute scattering by two attached cubes. The resulting particle is a square prism with an aspect ratio of 2:1. The model including the circumscribing spheres is depicted in Fig. 3. The diameter of the spheres is $\sqrt{3}$ times the edge length of the cubes. This leads to a significant overlap of the spheres. The intersecting volume of the two spheres is 62.6% of the volume of one basic cube.

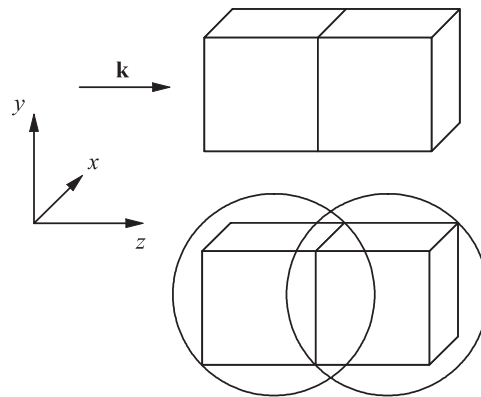


Fig. 3. Model of two attached cubes (top). The figure below shows the circumscribing spheres of the cubes. These spheres intersect where the cubes are attached. The cubes are aligned along the main axes. The incident direction is along the z-axis.

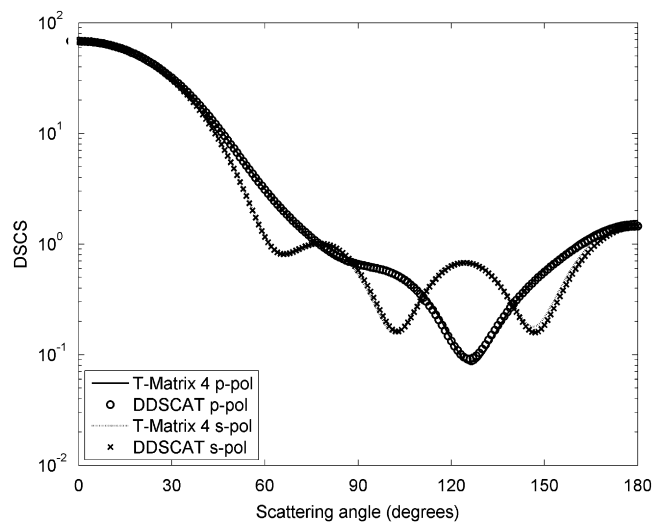


Fig. 4. Scattering diagram of two composite cubes depicted in Fig. 3. The size parameter of each cube is $kd = 4.0$. The refractive index is 1.5. The scattering results for the s- and the p-polarization are shown. The corresponding curves of the T-matrix and DDSCAT computations show good agreement.

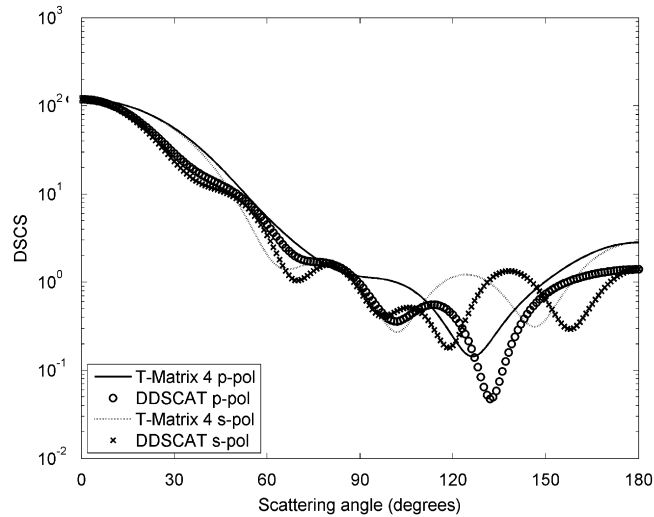


Fig. 5. Scattering diagram of two composite cubes depicted in Fig. 3. The size parameter of each cube is $kd = 5.6$. The refractive index is 1.5. The scattering results for the s- and the p-polarization are shown. The corresponding curves of the T-matrix and DDSCAT computations show visible deviations.

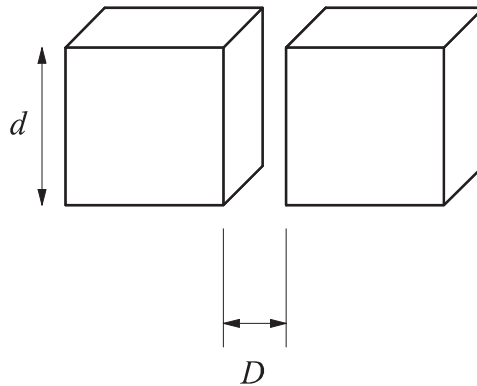


Fig. 6. Model of two separated cubes with the edge length d and the separation distance D .

Nevertheless, comparison of the DSCS computed with the T-matrix method and DDA shows good agreement up to a size parameter of $kd = 4.0$ of the basic cubes. From Fig. 4 it can be seen that the deviations are small and only visible in the backscattering region. Both the p- and s-polarizations show good agreement.

With a larger size parameter of $kd = 5.6$ as shown in Fig. 5, the comparison of the T-matrix and DDA computations shows strong deviations in the DSCS for both polarizations. It can be stated that the upper limit of the method is in the region where the size parameter of the basic cube is about $kd = 4.0$. Further computations show that the computational results can be acceptable even for a size parameter of $kd = 8.0$. But the accuracy of the method cannot be guaranteed.

6.2. Investigation of the influence of the distance between two cubes

We assume that there will be a better agreement between T-matrix and DDA computations if the overlapping volumes of the circumscribing spheres is reduced. According to the T-matrix theory, computation of multiple scattering is correct if the circumscribing spheres do not overlap. In the following we present computational results of two basic cubes that are separated by a distance D as shown in Fig. 6.

In Fig. 7 the scattering diagram of two separated cubes with the size parameter $kd = 5.6$ is shown. The separation distance is $kd = 1.4$. Thus, the circumscribing spheres still are overlapping. The intersection volume is still 17.7% of the volume of a cube. Nevertheless, the comparison of the T-matrix and DDA computations shows excellent agreement. Comparing the scattering diagrams of Figs. 5 and 7, it can be easily seen that there is a high influence of the overlapping circumscribing spheres. We have to stress that the size parameter of $kd = 5.6$ is already quite high for multiple scattering with nonaxisymmetric particles.

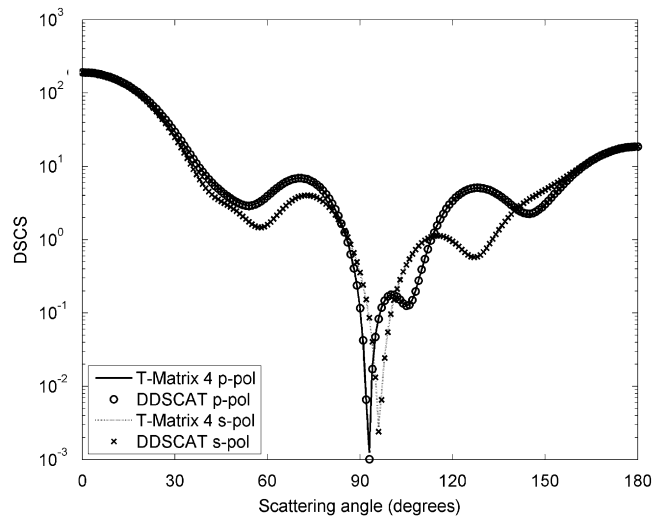


Fig. 7. Scattering diagram of two composite cubes with a separation distance as depicted in Fig. 6. The size parameter of each cube is $kd = 5.6$. The corresponding separation distance is $kd = 1.4$. The refractive index is 1.5. The scattering results for the s- and the p-polarization are shown. The corresponding curves of the T-matrix and DDSCAT computations show excellent agreement.

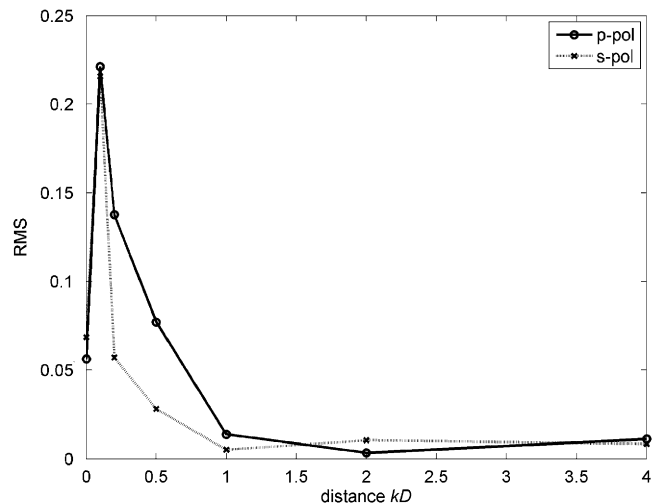


Fig. 8. Diagram of the RMS errors for two cubes depending on the separation distance kd . The size parameter of each of the two cubes is $kd = 4.0$.

In Figs. 8 and 9 we present the RMS error which indicates the deviations between T-matrix and DDA results in dependence on the separation distance kd between the two cubes. From both figures it can be seen that there are high RMS values for low separation distances. In Fig. 8 the RMS error for two cubes of the size parameter $kd = 4.0$ for p- and s-polarization is plotted. The separation distance of $kd = 0$ refers to the scattering diagram of Fig. 4. The RMS error reaches a maximum value of about 0.22 for the separation distance $kd = 0.1$. The RMS error of 0.22 still leads to very good agreement between the computational results of T-matrix and DDA. Only minor deviations in the backscattering region are visible. At a separation distance of $kd = 1.0$ and higher the agreement in the scattering diagrams is excellent.

In Fig. 9 we show the RMS error for two cubes of size parameter $kd = 5.6$. The separation distance of $kd = 0$ refers to the scattering diagram of Fig. 5. The RMS error reaches a maximum value for s-polarization of 0.7 and for p-polarization of 0.54 for the separation distance $kd = 0$. Acceptable RMS errors below 0.2 are only obtained for separation distances higher than $kd = 0.7$. There, only minor deviations in the backscattering region are visible. At a separation distance of $kd = 1.4$ and higher the agreement in the scattering diagrams is excellent.

6.3. Four cubes

The next model we would like to present is shown in Fig. 10. Four equally sized cubes are placed in a row forming a square prism with an aspect ratio of 4:1. The four circumscribing spheres of the cubes have three intersecting regions.

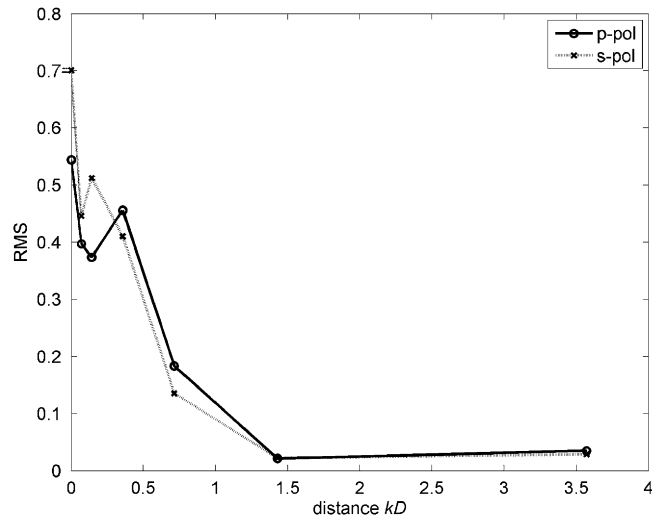


Fig. 9. Diagram of the RMS errors for two cubes depending on the separation distance kD . The size parameter of each of the two cubes is $kd = 5.6$.

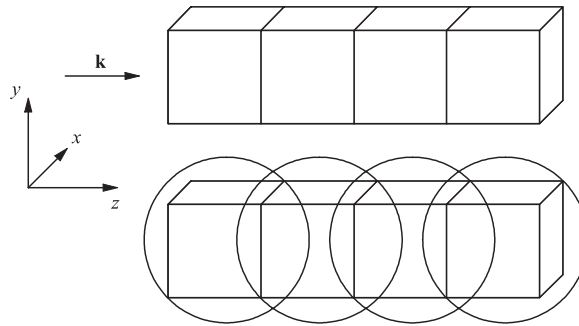


Fig. 10. Model of a square prism built-up of four cubes (top). The circumscribing spheres of the cubes are overlapping in three regions (bottom).

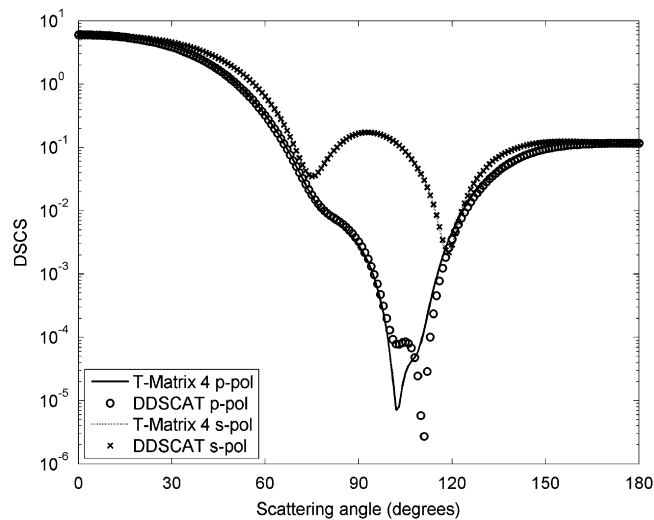


Fig. 11. Scattering diagram of the square prism consisting of four cubes as depicted in Fig. 10. The size parameter of each cube is $kd = 2.0$. The refractive index is 1.5. The scattering results for the s- and the p-polarization are shown. The corresponding curves of the T-matrix and DDSCAT computations show good agreement except for the p-polarization in the range of 90–110° of the scattering angle.

In the following we will present computational results of scattering by such a particle for different sizes and compare these results to the DDA solutions.

Scattering by a square prism with the size parameter of $kd = 2.0$ of the basic cubes is shown in Fig. 11. There is a good agreement between the T-matrix and DDA results except for the range of $100\text{--}120^\circ$ of the scattering angle. Only p-polarization is affected. In many cases this is acceptable since the DSCS in this range has small values.

In Fig. 12 we present the scattering diagrams of the same shape but with the size parameter of $kd = 4.0$ of the basic cube. T-matrix and DDA computational results show small deviations, mainly in the backscattering region. The deviations are less pronounced for s-polarization than for p-polarization.

The RMS error for the square prism with an aspect ratio of 4:1 in dependence on the size parameter kd of a single cube is shown in Fig. 13. It is notable that the RMS error for s-polarization is lower for all considered size parameters from $kd = 0.5\text{--}8.0$. The remarkable high value at $kd = 1.4$ for p-polarization can be explained by deviations in the range of the scattering angle between 80° and 110° where the DSCS shows low values. The same holds for the size parameters of $kd = 1.0$ and 2.0 (Fig. 11).

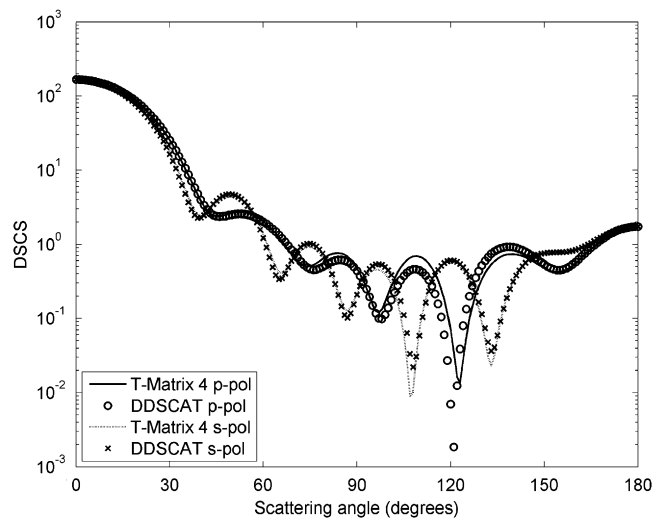


Fig. 12. Scattering diagram of the square prism consisting of four cubes as depicted in Fig. 10. The size parameter of each cube is $kd = 4.0$. The refractive index is 1.5. The scattering results for the s- and the p-polarization are shown. The corresponding curves of the T-matrix and DDSCAT computations show acceptable agreement with visible deviations in the range of $80\text{--}140^\circ$ of the scattering angle.

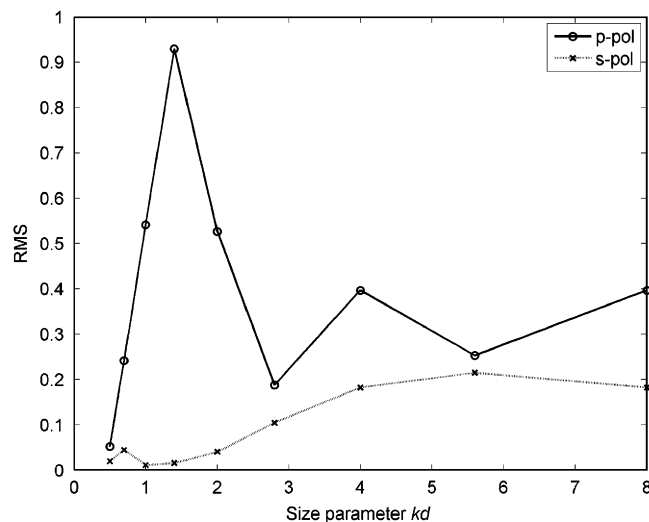


Fig. 13. Diagram of the RMS errors for the square prism (four cubes) depending on the size parameter kd of the basic cube. The two polarizations show a different behaviour.

The computation time is representatively shown for four attached cubes in Table 1. It can be seen that computation time is higher for the **T**-matrix method. The values are generally higher for the **T**-matrix method. On the other hand, the **T**-matrix method has a great advantage compared to the method of DDA. Once the **T**-matrix is computed, various orientations of the scattering object can be computed quickly. In addition, it is possible to compute the fully orientation averaged **T**-matrix quickly. This is not possible with the method of DDA, where most orientations of the particle require separate computations.

6.4. Cube composed of eight smaller cubes

Finally, we will present computational results of scattering by a cube which is composed of eight single cubes. The model with the corresponding circumscribing spheres is shown in Fig. 14.

An example of multiple scattering by these cubes as depicted in Fig. 14 is shown in Fig. 15. The size parameter of the basic cubes is $kd = 2.0$. For this reason, the composed cube has the size parameter of 4.0. Comparison of **T**-matrix and DDA

Table 1

Comparison of computation time between the **T**-matrix method and DDA for four attached cubes

| | Computation time | | | | | | |
|------------------------------------|------------------|------------|------------|------------|------------|------------|------------|
| | $kd = 1.0$ | $kd = 1.4$ | $kd = 2.0$ | $kd = 2.8$ | $kd = 4.0$ | $kd = 5.6$ | $kd = 8.0$ |
| T -matrix 4 cubes (s) | 5 | 6 | 101 | 803 | 1300 | 707 | 8602 |
| DDSCAT 4 cubes (s) | 0.37 | 1.3 | 4.8 | 24.5 | 124 | 231 | 584 |
| T -matrix of basic cube (s) | 0.62 | 0.61 | 2.3 | 32 | 80 | 166 | 1514 |

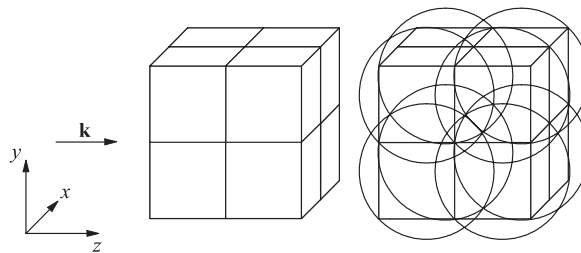


Fig. 14. Model of a cube composed of eight smaller cubes (left). The figure on the right shows the circumscribing spheres of the cubes. Each sphere shows multiple intersection regions where the cubes are connected.

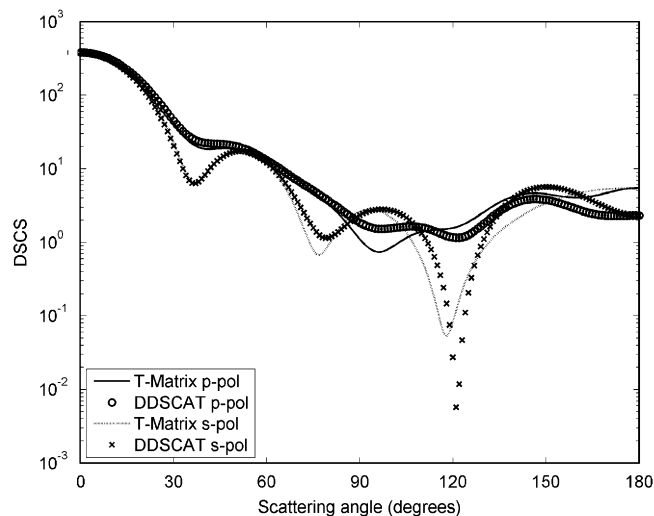


Fig. 15. Scattering diagram of the cube consisting of eight cubes as depicted in Fig. 14. The size parameter of each cube is $kd = 2.0$. The refractive index is 1.5. The scattering results for the s- and the p-polarization are shown. The corresponding curves of the **T**-matrix and DDSCAT computations show good agreement except for the p-polarization in the range of 90–110° of the scattering angle.

computational results shows good agreement in the DSCS. Again, the deviations are smaller for p-polarization. In the region of the scattering angle from 90° to 120° there are visible deviations for s-polarization. Nevertheless, the absolute values of the DSCS in this region reach a minimum.

In Fig. 16 the DSCS of a composed cube with the size parameter of 8.0 is shown. The basic cubes have a size parameter of $kd = 4.0$. The deviations between T-matrix and DDA computations are clearly visible, they are mainly in the backscattering region. The forward scattering direction up to a scattering angle of 60° shows good agreement between both methods.

In Fig. 17 the RMS error for the composed cube over a wide range of the size parameter kd of the basic cubes is shown. Due to the multiple overlapping of the circumscribing spheres, the comparison between T-matrix and DDA computations shows good results for only low size parameters. Good agreement could only be reached for the size parameters of $kd = 0.5$ and 2.0 of the basic cubes. The cases of $kd = 0.7, 1.0,$ and 1.4 show acceptable deviations for the s-polarization but strong deviations for the p-polarization. In the range of the size parameter $2 \leq kd \leq 8$ the RMS error is increasing steadily where the RMS value is lower for the p-polarization.

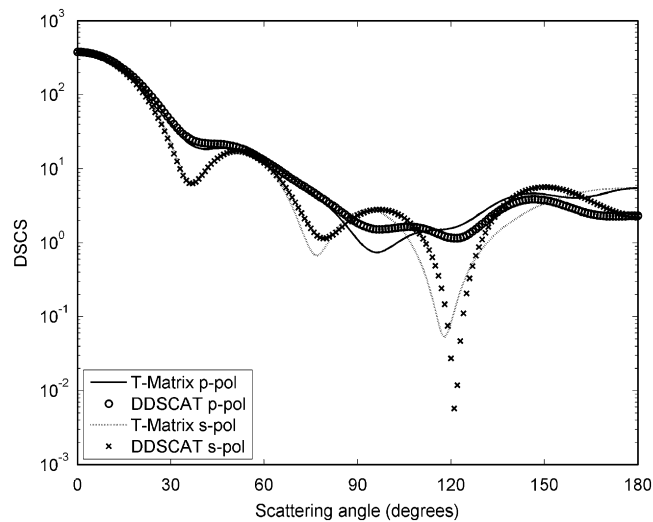


Fig. 16. Scattering diagram of the cube consisting of eight cubes as depicted in Fig. 14. The size parameter of each cube is $kd = 4.0$. The refractive index is 1.5. The scattering results for the s- and the p-polarization are shown. The corresponding curves of the T-matrix and DDSCAT computations show good agreement only for scattering angles below 60° . For scattering angles over 60° the deviations are clearly visible.

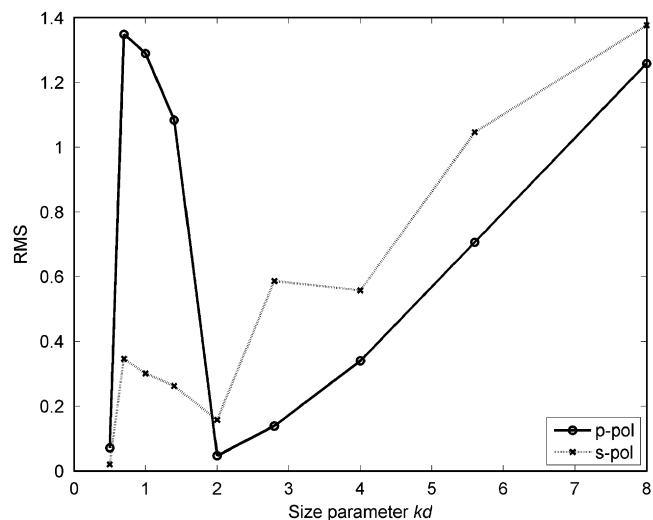


Fig. 17. Diagram of the RMS errors for the cube consisting of eight cubes depending on the size parameter kd of the basic cube. The two polarizations show a different behaviour.

7. Conclusion

A new method for computation of the **T**-matrix of composed nonaxisymmetric particles is presented. The method is based on decomposition of a particle into smaller basic particles. A multiple scattering approach using the null-field method with discrete sources (NFM-DS) is used. This approach allows the computation of the **T**-matrix of a particle which is composed of smaller particles for which the **T**-matrix is easier to compute. In this paper we concentrated on cubes as basic particles. By using multiple scattering of cubes, the **T**-matrix of particle shapes can be computed which is difficult to get by conventional methods.

Computation results are compared for the two methods, NFM-DS and DDA. We show different examples of particles, which consist of two, four, and eight cubes, and present computational results. The RMS error is examined in order to prove the validity of the method. We could show that the error can be associated with the overlapping of the circumscribing spheres. Nevertheless, the example of the square prism demonstrates good computational results up to a size parameter of $kd = 2.8$. The example of the cube composed of eight smaller cubes shows good results up to a size parameter of $kd = 2.0$. In both cases, the p-polarization shows higher deviation and can be explained by the lower values of the DSCS. The limits of the size parameter cannot be generalized to other geometries, especially using more complex geometries like aggregated platelets, torus, or helix shaped particles. In each case, a detailed analysis of the RMS error should be considered.

Acknowledgement

We would like to acknowledge support of this research by DFG (Deutsche Forschungsgemeinschaft).

References

- [1] Mishchenko MI, Videen G, Babenko VA, Khlebtsov NG, Wriedt T. *T*-matrix theory of electromagnetic scattering by particles and its applications: a comprehensive reference database. *JQSRT* 2004;88:357–406.
- [2] Mishchenko MI, Videen G, Babenko VA, Khlebtsov NG, Wriedt T. Comprehensive *T*-matrix reference database: a 2004–2006 update. *JQSRT* 2007;106:304–24.
- [3] Peterson B, Ström S. *T*-matrix for electromagnetic scattering from an arbitrary number of scatterers and representations of $E(3)$. *Phys Rev* 1973;8:3661–78.
- [4] Xu YL. Radiative-scattering signatures of an ensemble of nonspherical particles. *JQSRT* 2004;89(1–4):385–419.
- [5] Wriedt T. Using *T*-matrix method for light scattering computations by non-axisymmetric particles: superellipsoids and realistically shaped particles. *Part Part Syst Charact* 2002;19:256–68.
- [6] Zhang L, Ruh E, Grützmacher D. Anomalous coiling of SiGe/Si and SiGe/Si/Cr helical nanobelts. *Nano Lett* 2007;6(7):1311–7.
- [7] Wiley BJ, Chen Y, McLellan JM, Xiong Y, Li Z-Y, Ginger D, et al. Synthesis and optical properties of silver nanobars and nanorice. *Nano Lett* 2007;7(4):1032–6.
- [8] Nehl CL, Liao H, Hafner JH. Optical properties of star-shaped gold nanoparticles. *Nano Lett* 2007;6(4):683–8.
- [9] Lu X, Au L, McLellan J, Li Z-Y, Marquez M, Xia Y. Fabrication of cubic nanocages and nanoframes by dealloying Au/Ag alloy nanoboxes with an aqueous etchant based on $\text{Fe}(\text{NO}_3)_3$ or NH_4OH . *Nano Lett* 2007;7(6):1764–9.
- [10] Doicu A, Wriedt T, Eremin Y. Light scattering by systems of particles null-field method with discrete sources—theory and programs. Berlin, Heidelberg, New York: Springer; 2006.
- [11] Wriedt T, Doicu A. *T*-matrix method for light scattering from particles on or near an infinite surface. In: Moreno F, González F, editors. *Light scattering from microstructures*. Berlin: Springer; 2000. p. 113–32.
- [12] Wriedt T, Schuh R, Doicu A. Scattering by aggregated fibres using a multiple scattering *T*-matrix approach. *Part Part Syst Charact* 2008;25:74–83.
- [13] Draine BT, Flatau PJ. User guide to the discrete dipole approximation code DDSCAT 6.1. URL: (<http://arxiv.org/abs/astro-ph/0409262>), 2004.
- [14] Wriedt T. Studies of light scattering by complex particles using the null-field method with discrete sources. In: Kokhanovsky AA, editor. *Light scattering reviews*, vol. 2. Berlin: Springer Praxis; 2007.
- [15] Peterson B, Ström S. Matrix formulation of acoustic scattering from an arbitrary number of scatterers. *J Acoust Soc Am* 1974;56:771–80.